Carboxymethyl Cellulose Sodium for Selective Depression of Fine-Grained Apatite from Chlorite and Biotite and Its Particle Size Effect

Mingmei Li , Libing Zhao * , Zurong Yi , Zixuan Yang , Jindong Han , Bin Guo , Ming Han , Wantao Li , Youbang Lai , Chuntao Wu , Xiaofei Guo

Posted Date: 23 April 2026

doi: 10.20944/preprints202604.1645.v1

Keywords: carboxymethyl cellulose sodium; apatite; chlorite; biotite; depressant; particle size effect

 doi:10.20944/preprints202604.1645.v1

Article

Carboxymethyl Cellulose Sodium for Selective Depression of Fine-Grained Apatite from Chlorite and Biotite and Its Particle Size Effect

Mingmei Li [1], Libing Zhao [1,*], Zurong Yi [1], Zixuan Yang [1], Jindong Han [1], Bin Guo [2], Ming Han [2], Wantao Li [2], Youbang Lai [2], Chuntao Wu [2] and Xiaofei Guo [3]

[1] School of Mining Engineering, North China University of Science and Technology, Tangshan 063210, Hebei, China

[2] HBIS Group Mining Co., Ltd., Tangshan 063000, Hebei, China

[3] School of Mining Engineering, University of Science and Technology Liaoning, Anshan 114051, Liaoning, China

* Correspondence: zlb2002@ncst.edu.cn

Abstract

To address the challenge of separating fine-grained apatite from layered silicate gangue minerals (chlorite and biotite) in medium-low grade collophanite ores, this study systematically investigated the effect of carboxymethyl cellulose sodium (CMC-Na) as a selective depressant on flotation behavior of different particle size fractions and its underlying mechanism. Pure mineral and artificial mixed ore flotation experiments demonstrated that at pH 9 and collector dosage of 5 kg/t, CMC-Na enabled selective separation of apatite from gangue minerals, with optimal dosage showing significant particle size effects: for the -0.5+0.074 mm fraction, effective separation was achieved with collector alone; for the -0.074+0.023 mm fraction, the optimal CMC-Na dosage was 10~100 mg/L, yielding 87% apatite recovery for pure minerals and 41.8% recovery with 23.7% P_2O_5 grade for mixed ores; for the -0.023 mm fine fraction, the optimal dosage was 30~300 mg/L, achieving 24.8% recovery and 13.2% grade. Mechanism studies revealed that CMC-Na significantly enhanced the hydrophilicity of chlorite and biotite, enlarging their surface property differences with apatite. FTIR and XPS analyses indicated that CMC-Na adsorbed on biotite via ion exchange with interlayer K^+ and coordination with octahedral Fe^{2+}/Mg^{2+}, and on chlorite through chemical coordination with octahedral Mg^{2+}, whereas only weak physical adsorption occurred on apatite surface Ca^{2+}. The adsorption strength followed the order: biotite > chlorite > apatite. This study provides an effective reagent scheme and theoretical basis for flotation separation of fine-grained phosphate ores.

Keywords: carboxymethyl cellulose sodium; apatite; chlorite; biotite; depressant; particle size effect

1. Introduction

China possesses abundant phosphate rock resources; however, approximately 80% of these reserves consist of medium-low grade collophanite (sedimentary phosphorite). With the continuous exploitation of mineral resources, high-grade and easily beneficiated phosphate ore reserves have been sharply depleted. The characteristics of phosphate ores have gradually deteriorated, exhibiting declining grades, fine dissemination particle sizes [1], and complex intergrowth relationships [2–4], thereby intensifying the flotation difficulties of medium-low grade phosphate ores. Chlorite and biotite are typical magnesium-, iron-, and aluminum-bearing layered silicate gangue minerals in phosphate ores. They readily slime, triggering complex interactive effects such as mutual adhesion and coating among minerals, which adversely affect flotation performance [5–7]. Conventional depressants such as sodium silicate demonstrate poor selectivity toward these minerals, require high

 doi:10.20944/preprints202604.1645.v1

dosages, and often cause difficulties in tailings settling [8,9]. Therefore, developing highly efficient and selective depressants targeting the structural characteristics of layered silicates and optimizing flotation separation processes represent critical research directions for achieving quality improvement and impurity reduction in phosphate concentrates, as well as ensuring the sustainable development of the phosphate chemical industry [10,11].

Flotation is a commonly employed technique for separating apatite from gangue minerals [12,13]. However, traditional flotation processes often encounter challenges when treating such ores, including low separation efficiency, high reagent consumption, and unsatisfactory concentrate grades. These problems largely stem from the significantly different flotation behaviors of minerals across various particle size fractions: coarse particles tend to detach from bubble surfaces due to their greater mass, while fine particles are prone to non-selective coating, severely interfering with the separation process [14–16]. Studies have shown that pre-classification of feed ore, directing different size fractions into appropriate reagent regimes and flotation circuits, can effectively mitigate interferences between particle sizes [17]. Consequently, classified flotation technology can substantially enhance overall flotation performance, reduce reagent consumption, and lower production costs, garnering increasing attention in the separation of high-ash difficult-to-float coal slimes and complex polymetallic ores [18–20].

Carboxymethyl cellulose sodium (CMC-Na), an anionic polysaccharide polymer, exhibits strong water solubility, abundant hydroxyl and carboxyl functional groups, and environmentally friendly characteristics, demonstrating potential application value in mineral flotation separation [21–24]. Research indicates that CMC-Na can adsorb onto mineral surfaces through hydrogen bonding, electrostatic interaction, and hydrophobic association, thereby altering surface hydrophilicity and effectively and selectively depressing certain gangue minerals [25–27].

In this study, CMC-Na was selected as the depressant, combined with a mixed collector system comprising sodium oleate, oxidized paraffin soap, and fatty acid methyl ester sulfonate. Through pure mineral and artificial mixed ore flotation experiments, the influence of CMC-Na on the classified flotation behavior of apatite, chlorite, and biotite was systematically investigated. Furthermore, modern characterization techniques including contact angle measurement, Zeta potential analysis, Fourier transform infrared spectroscopy (FTIR), and X-ray photoelectron spectroscopy (XPS) were comprehensively employed to elucidate the adsorption mechanism of CMC-Na on the three mineral surfaces.

2. Materials and Methods

2.1. Test Samples and Reagents

The pure mineral samples of apatite, chlorite, and biotite used in this study were obtained from Lianyungang, Jiangsu Province, China. High-crystallinity ore blocks were selected, crushed, manually sorted to remove impurities, and ground. Wet sieving with standard screens was then conducted to obtain four size fractions: +0.5 mm, 0.5–0.074 mm, 0.074–0.023 mm, and −0.023 mm. The coarse +0.5 mm fraction was reserved for future use, while the remaining three fractions were employed for subsequent flotation tests. Artificial mixed ore samples were prepared by mixing pure apatite, pure chlorite, and pure biotite at a mass ratio of 1:1:1.

X-ray fluorescence spectroscopy (XRF) and X-ray diffraction (XRD) were used to analyze the chemical composition and mineralogical phases of the pure apatite and calcite minerals. The results are presented in Tables 1–3 and Figure 1. The analyses indicated that the apatite was fluorapatite with a calculated purity of 96%; the chlorite sample had a calculated purity of 95%; and the biotite sample achieved a calculated purity of 98%. The XRD patterns showed only characteristic diffraction peaks of apatite, chlorite, and biotite, with no diffraction peaks from other impurity minerals detected, confirming that the sample purities met the requirements for pure mineral flotation experiments.

Sodium oleate (analytical grade, ≥98% purity, Tianjin Huasheng Chemical Reagent Co., Ltd., Tianjin, China), oxidized paraffin soap (analytical grade, mixture without single purity value, quality

 doi:10.20944/preprints202604.1645.v1

conforming to manufacturer's analytical grade specifications, Guangdong Yuanfeng Chemical Reagent Co., Ltd., Guangdong, China), and sodium fatty acid methyl ester sulfonate (industrial grade, 85% purity, Shanghai Macklin Biochemical Co., Ltd., Shanghai, China) were mixed in certain proportions to prepare the collector for apatite flotation. CMC-Na (analytical grade, ≥95% purity, Tianjin Kemiou Chemical Reagent Co., Ltd., Tianjin, China) was used as the depressant for apatite flotation. Deionized water with resistivity greater than 18.2 MΩ·cm was used for all test solution preparation and flotation processes.

Table 1. Chemical composition analysis of pure apatite.

Name	CaO	P_2O_5	F	SiO_2	SO_3	Fe_2O_3	SrO	MgO	MnO
Content	56.51	38.58	1.53	1.10	0.85	0.09	0.07	0.04	0.04

Table 2. Chemical composition analysis of pure chlorite.

Name	SiO_2	Al_2O_3	Fe_2O_3	MgO	CaO	Na_2O	K_2O	MnO	TiO_2
Content	32.54	18.32	9.91	26.87	1.82	0.14	0.01	0.06	0.33

Table 3. Chemical composition analysis of pure biotite.

Name	IL	Al_2O_3	SiO_2	Fe_2O_3	CaO	MgO	K_2O	Na_2O	TiO_2
Content	2.06	17.10	40.72	13.95	0.18	15.88	8.82	0.10	0.89

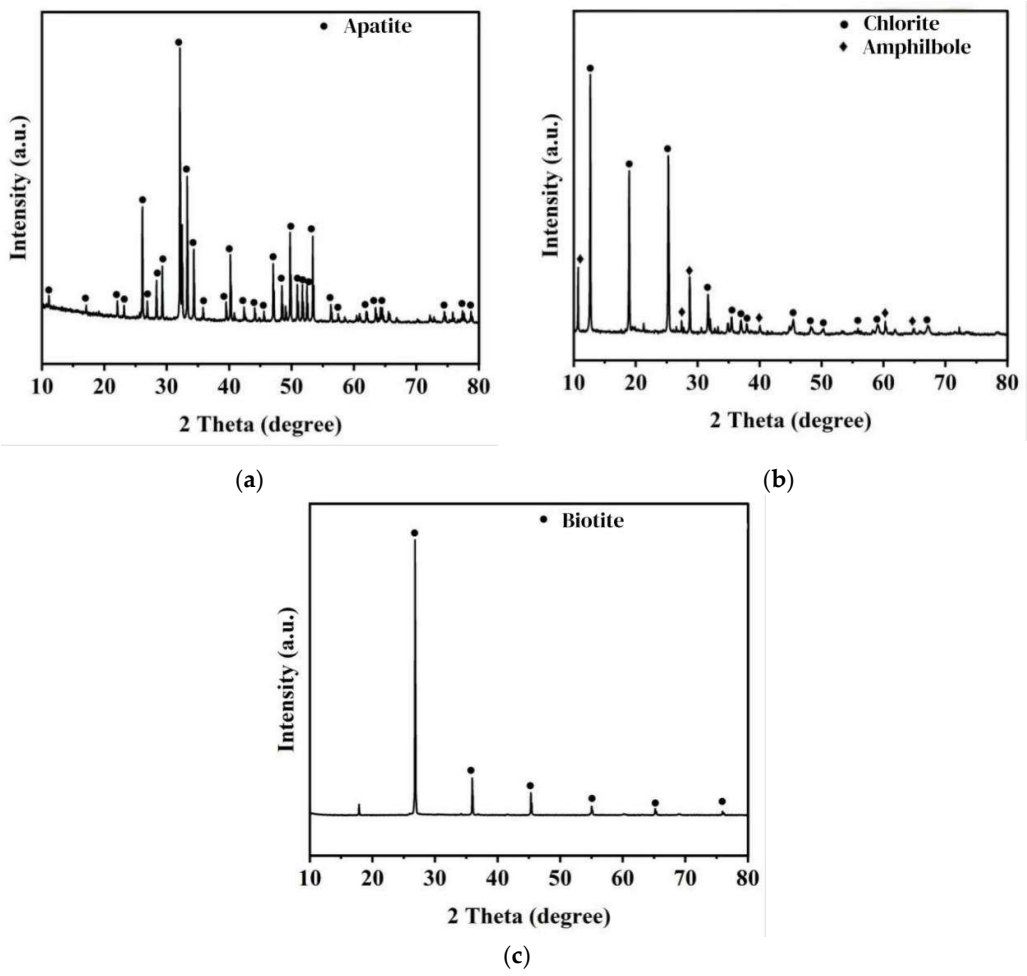

Figure 1. XRD patterns of apatite, chlorite, and biotite:(a) Apatite; (b)Chlorite;(c)Biotite.

 doi:10.20944/preprints202604.1645.v1

2.2. Experimental Methods

2.2.1. Single Mineral Flotation Tests

The flotation separation tests of apatite from gangue minerals (chlorite and biotite) were divided into pure mineral flotation tests and artificial mixed ore flotation tests. Both were conducted in a 50 mL hanging trough flotation cell following identical experimental procedures.

The experimental procedure was as follows: (1) Accurately weigh 2.0 g of sample and mix with 40 mL deionized water in the flotation cell. (2) Set the flotation machine speed to 1992 rpm and stir for 2 min. (3) Add dilute HCl or NaOH solution to adjust to the target pH value. (4) Stir for 2 min. (5) Add CMC-Na inhibitor solution according to the set concentration gradient. (6) Stir for 3 min. (7) Add the collector. (8) Stir for 3 min. (9) Conduct aeration and scrape the froth for 3 min. (10) Filter the froth product using quantitative filter paper and dry in an oven at 70°C. (11) Weigh the obtained concentrate and calculate the yield and recovery. (12) For artificial mixed ore tests, the concentrate product was further subjected to P_2O_5 grade analysis.

2.2.2. Reagent Mechanism Detection and Analysis

(1) Contact Angle Measurement

An appropriate amount of fully dried apatite and calcite powder was pressed into a flat and dense sheet sample under specific pressure and fixed on the sample stage of a contact angle measuring instrument. The three-dimensional platform was precisely adjusted to ensure that the sample surface was horizontal and parallel to the optical axis of the lens. Approximately 2 μL of ultrapure water droplet was deposited on the sample surface using a micro-injection unit. The droplet morphology was recorded in real-time through a high-speed camera system, and the static contact angle value was calculated by fitting with the Young-Laplace equation [28,29].

(2) Zeta Potential Measurement

Zeta potential was measured using a Zeta potential analyzer. 1.0 g of pure mineral sample with particle size of −0.023 mm was weighed and placed in a beaker, and 20 mL of ultrapure water was added. The sample was fully dispersed by magnetic stirring. The pulp pH was precisely adjusted to 7, 8, 9, 10, 11, and 12 using dilute HCl or NaOH solution. At each preset pH point, the pulp was divided into two equal portions: one as a blank control and the other with a quantitative amount of inhibitor solution added. Both groups of samples were continuously stirred for 20 min to ensure full interaction between the reagent and minerals, then centrifuged to obtain the supernatant for Zeta potential measurement [30].

(3) Fourier Transform Infrared Spectroscopy (FTIR) Detection

1.0 g of pure mineral sample with particle size of −0.023 mm was weighed and placed in a beaker containing 20 mL of ultrapure water, dispersed by magnetic stirring. A quantitative amount of inhibitor solution was added to the pulp and stirred for an additional 20 min. After the reaction was completed, the pulp was filtered using medium-speed quantitative filter paper. The obtained filter cake was thoroughly dried in a constant temperature oven at 105°C. The dried sample was fully ground and mixed with spectroscopically pure potassium bromide (KBr) at a mass ratio of 1:100 in an agate mortar, then pressed into a transparent thin sheet. Finally, the Fourier transform infrared spectrometer was used to collect infrared spectra in the wavelength range of 4000–400 cm^{-1} in transmission mode.

(4) X-ray Photoelectron Spectroscopy (XPS) Detection

Pure mineral samples of apatite, chlorite, and biotite treated with and without inhibitor were selected for surface elemental composition and chemical state analysis using an X-ray photoelectron spectrometer. The collected high-resolution spectra of C 1s, Ca 2p, Mg 1s, K 2p, and other elements were subjected to peak fitting processing using the instrument's supporting Avantage software to analyze the adsorption mechanism of the inhibitor on the mineral surfaces.

 doi:10.20944/preprints202604.1645.v1

3. Results and Discussion

3.1. Flotation Tests

3.1.1. Collector Dosage Tests

Flotation separation of three minerals with different particle sizes was conducted at natural pH, and the results are shown in Figures 2, 3, and 4:

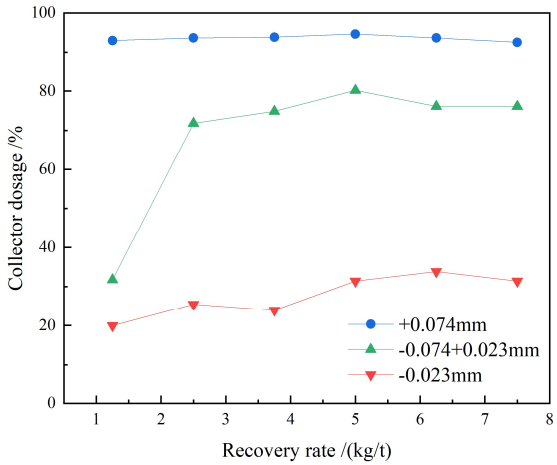

Figure 2. Effect of collector dosage on flotation performance of different particle size fractions of apatite.

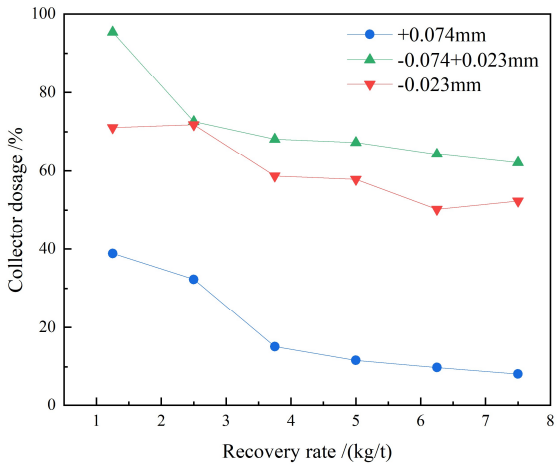

Figure 3. Effect of collector dosage on flotation performance of different particle size fractions of chlorite.

 doi:10.20944/preprints202604.1645.v1

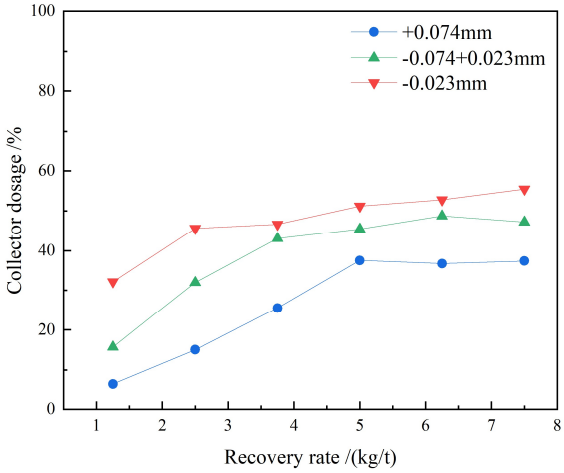

Figure 4. Effect of collector dosage on flotation performance of different particle size fractions of biotite.

As shown in Figure 2, the flotation behavior of apatite varies across different particle size fractions: the coarse fraction (+0.074 mm) maintains consistently high recoveries of 93% – 95%, essentially unaffected by collector dosage; the medium-fine fraction (−0.074+0.023 mm) shows a positive correlation between recovery and dosage, reaching a peak of 80% at 5 kg/t; the fine fraction (−0.023 mm) maintains a stable recovery of 33% within the 5 – 7.5 kg/t range. As illustrated in Figures 2 and 3, the recovery of the gangue mineral chlorite decreases with increasing reagent dosage across all size fractions, while biotite recovery shows a slight increase with dosage but remains below 60%. Considering the recovery efficiency of the target mineral, the depression effect on gangue minerals, and economic costs, the optimal collector dosage was determined to be 5 kg/t, which achieves efficient selective recovery of apatite while maintaining production economy.

3.1.2. pH Determination

The effect of different pH values on mineral flotation was investigated under pH 5–11 conditions, and the results are shown in Figures 5, 6, and 7.

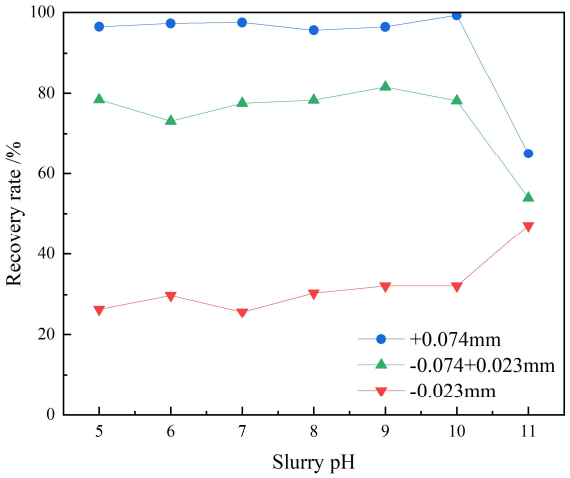

Figure 5. Effect of pH on flotation performance of different particle size fractions of apatite.

 doi:10.20944/preprints202604.1645.v1

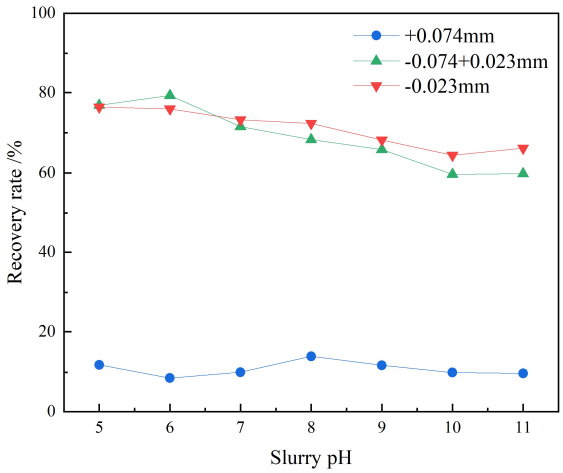

Figure 6. Effect of pH on flotation performance of different particle size fractions of chlorite.

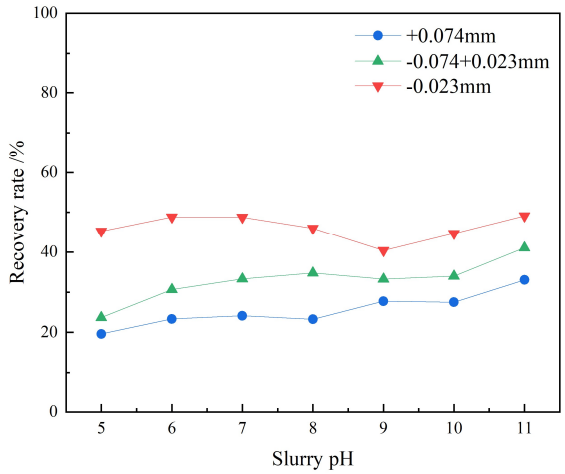

Figure 7. Effect of pH on flotation performance of different particle size fractions of biotite.

As shown in Figures 5, 6, and 7, in neutral or weakly alkaline environments, the recovery of +0.074 mm fraction apatite remains consistently stable at a high level above 95%, while the recoveries of gangue minerals chlorite and biotite are maintained at relatively low levels, with chlorite recovery ranging between 8% and 14%, and biotite recovery between 19% and 28%. This significant difference in recovery rates enables effective separation of the target mineral from gangue minerals in this size fraction without the need for additional depressants. Therefore, subsequent experiments on depressants and dispersants will focus on the −0.074+0.023 mm and −0.023 mm size fractions.

A pulp pH of 9 achieves optimal selective separation. This condition ensures effective recovery of apatite while maximizing the depression of gangue minerals.

3.1.3. CMC-Na Dosage Tests

Under the conditions of pH 9 and collector dosage of 5 kg/t, the flotation test results of −0.074+0.023 mm and −0.023 mm fractions of apatite, chlorite, and biotite at different CMC-Na dosages are shown in Figures 8 and 9.

 doi:10.20944/preprints202604.1645.v1

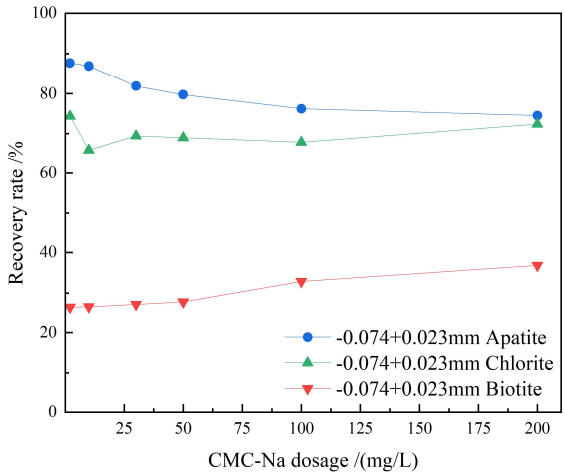

Figure 8. Effect of CMC-Na on floatability of −0.074+0.023 mm frraction apatite, chlorite, and biotite.

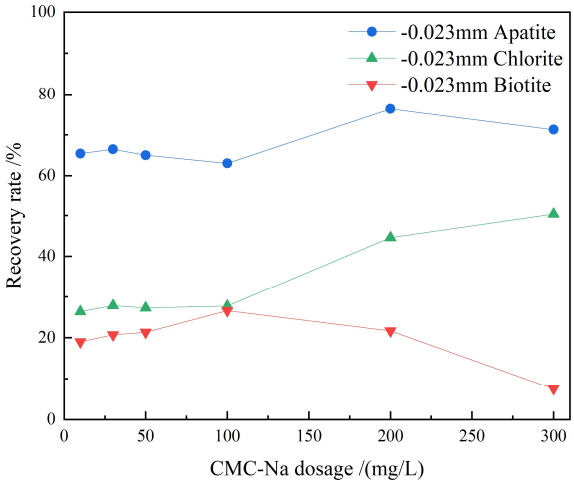

Figure 9. Effect of CMC-Na on floatability of −0.023 mm frraction apatite, chlorite, and biotite.

As shown in Figure 8, for the −0.074+0.023 mm size fraction of the three minerals, a low CMC-Na dosage (10 mg/L) is most favorable for apatite flotation, with the highest recovery reaching 87%, followed by a slight decrease and stabilization at approximately 74% with increasing dosage. The recovery of chlorite first decreases and then increases, reaching a minimum of 65% at 10 mg/L, and then slowly recovering to approximately 70%. Biotite exhibits the poorest floatability, with recovery gradually increasing from 26% to 41% as reagent dosage increases. Overall, the optimal separation of the three minerals is achieved at a CMC-Na dosage of 10 mg/L.

As shown in Figure 9, for the −0.023 mm size fraction, significant differences in recovery between apatite and chlorite/biotite are observed at lower CMC-Na concentrations. Apatite recovery remains stable at approximately 66% in the 20–50 mg/L range, then rises to 76% before declining to 71%. Chlorite recovery remains stable at approximately 30% in the 20–100 mg/L range, and then significantly increases to 50% with further increase in reagent dosage. Biotite recovery shows a "first increase then decrease" trend, briefly declining at 50 mg/L before recovering, reaching a peak at 100 mg/L, and subsequently decreasing. Considering separation efficiency and economy, the optimal CMC-Na dosage was determined to be 30 mg/L.

Pure mineral tests indicate that the selective depression capability of CMC-Na on chlorite, biotite, and apatite is related not only to particle size but also to dosage.

 doi:10.20944/preprints202604.1645.v1

3.1.4. Artificial Mixed Mineral Tests

Under the conditions of pH 9 and collector dosage of 5 kg/t, the effect of CMC-Na dosage on the separation of different particle size fractions of apatite from chlorite and biotite (mixed at a mass ratio of 1:1:1) was further investigated, and the results are shown in Figures 10 and 11.

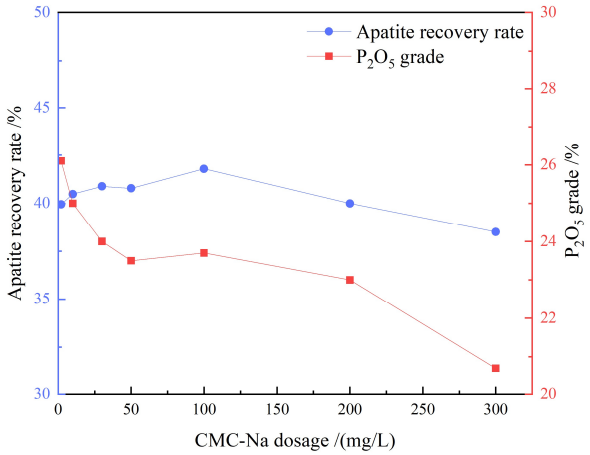

Figure 10. Effect of CMC-Na on mixed flotation of −0.074+0.023 mm fraction apatite, chlorite, and biotite.

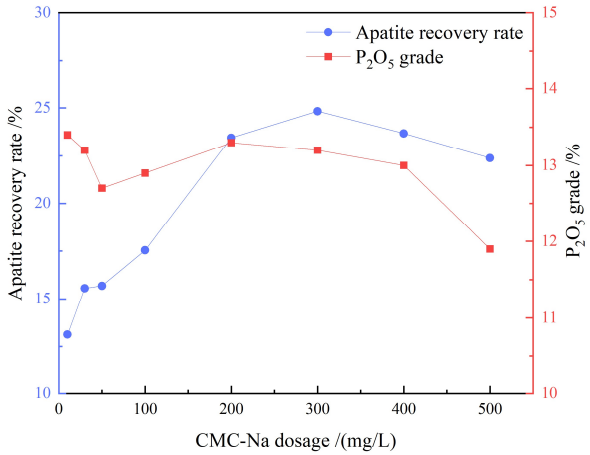

Figure 11. Effect of CMC-Na on mixed flotation of −0.023 mm fraction apatite, chlorite, and biotite.

As shown in Figure 10, CMC-Na dosage has a significant effect on the flotation performance of different particle size fractions of apatite. For the −0.074+0.023 mm size fraction, recovery reaches a peak of 41.8% at 100 mg/L, while the grade continues to decline. Considering both factors, 100 mg/L was determined as the optimal dosage, where recovery and grade (23.7%) are most balanced. As shown in Figure 11, for the −0.023 mm fine size fraction, recovery is highest (24.8%) at 300 mg/L, while the grade is highest (13.4%) at 10 mg/L; however, the comprehensive index is optimal at 300 mg/L (recovery 24.8%, grade 13.2%). At low dosages, CMC-Na preferentially depresses gangue minerals, enhancing selectivity; at high dosages, it adsorbs onto the apatite surface, depressing its floatability and resulting in decreased recovery and grade.

 doi:10.20944/preprints202604.1645.v1

3.2. Mechanism Analysis

3.2.1. Contact Angle Measurements

The surface contact angle measurement results of apatite, chlorite, and biotite after interaction with reagents are shown in Figures 12, 13, and 14.

(**a**) (**b**)

Figure 12. Contact angle of apatite before and after CMC-Na interaction: (**a**) Apatite+Collector; (**b**) Apatite+CMC-Na+Collector.

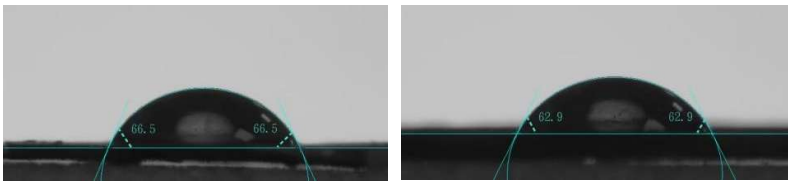

(**a**) (**b**)

Figure 13. Contact angle of chlorite before and after CMC-Na interaction: (**a**) Chlorite+Collector; (**b**) Chlorite+CMC-Na+Collector.

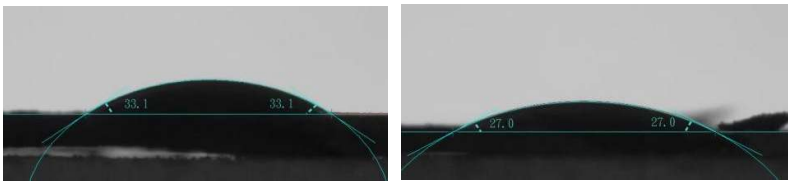

(**a**) (**b**)

Figure 14. Contact angle of biotite before and after CMC-Na interaction: (**a**) Biotite+Collector; (**b**) Biotite+CMC-Na+Collector.

As shown in Figure 12, after the addition of the depressant CMC-Na, the target mineral apatite maintains strong floatability despite a slight decrease in hydrophobicity (contact angle from 85.7° to 75.3°). As shown in Figures 13 and 14, the gangue minerals are significantly depressed, with the contact angles of chlorite and biotite decreasing to 62.9° and 27.0°, respectively, indicating substantially enhanced hydrophilicity. The reagent regime effectively enlarges the wettability difference between apatite and gangue minerals (particularly biotite), providing the essential surface property basis for preferential flotation separation of apatite.

3.2.2. Zeta Potential Analysis

The Zeta potential variation curves of apatite, chlorite, and biotite with pH before and after interaction with CMC-Na are shown in Figures 15, 16, and 17.

 doi:10.20944/preprints202604.1645.v1

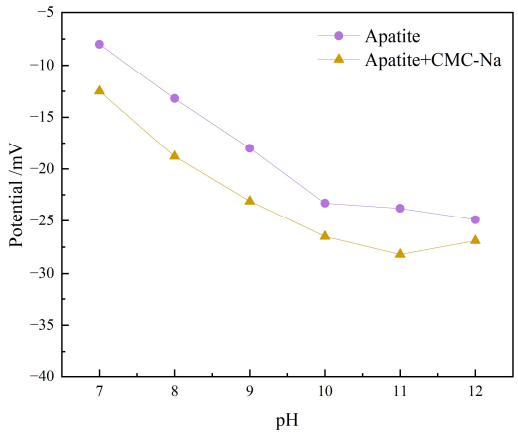

Figure 15. Zeta potential of apatite before and after CMC-Na interaction.

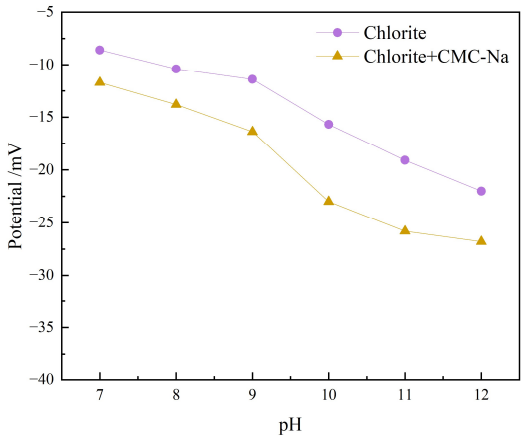

Figure 16. Zeta potential of chlorite before and after CMC-Na interaction.

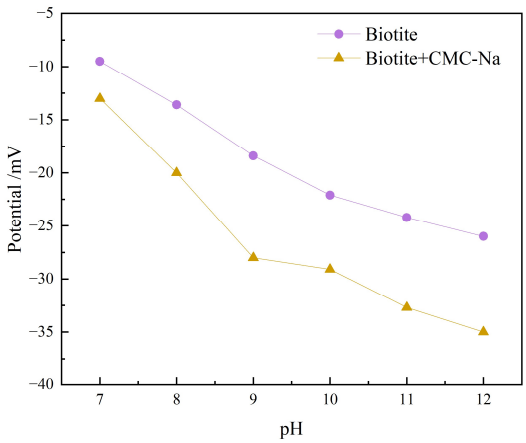

Figure 17. Zeta potential of biotite before and after CMC-Na interaction.

Figures 15, 16, and 17 show that the adsorption strength of CMC-Na follows the order: biotite > chlorite > apatite, with negative shifts of −9.5, −7.5, and −6.0 mV, respectively, confirming its stronger adsorption on gangue minerals. Biotite exhibits continuous strong adsorption in the pH 9–12 range due to interlayer K^+ exchange and surface coordination; chlorite reaches its adsorption peak at pH 10; while apatite shows weakened adsorption after pH 8. The pH 9–10 range represents the optimal

 doi:10.20944/preprints202604.1645.v1

separation window, where the maximum potential difference between gangue minerals and apatite enables selective depression.

3.2.3. FTIR Analysis

FTIR detection was performed on apatite, chlorite, and biotite before and after CMC-Na treatment, and the results are shown in Figures 18, 19, and 20.

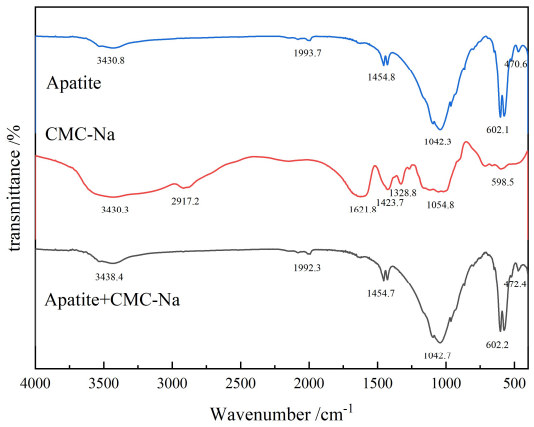

Figure 18. FTIR spectra of apatite before and after CMC-Na interaction.

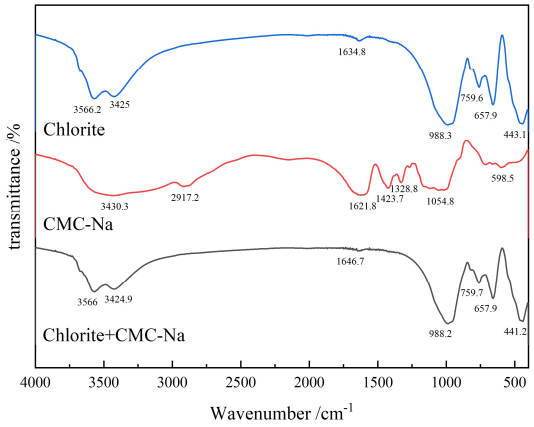

Figure 19. FTIR spectra of chlorite before and after CMC-Na interaction.

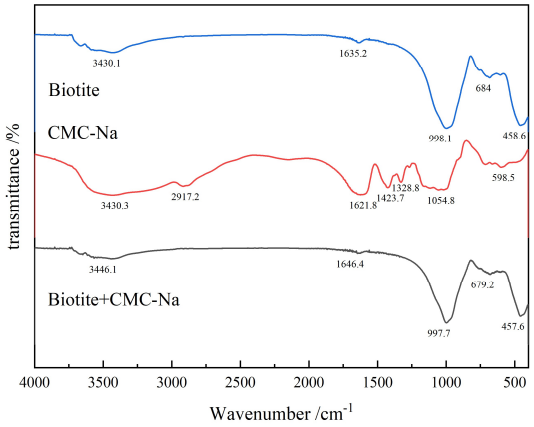

Figure 20. FTIR spectra of biotite before and after CMC-Na interaction.

 doi:10.20944/preprints202604.1645.v1

Figures 18, 19, and 20 confirm that the adsorption strength of CMC-Na on the three minerals follows the order: biotite > chlorite > apatite. The characteristic C=O stretching peak of the carboxylate group in CMC-Na (~1621 cm^{-1}) consistently shifts to higher wavenumbers (to ~1646–1647 cm^{-1}) after mixing, indicating coordination between the carboxyl groups and metal ions on the mineral surfaces. Biotite exhibits the strongest 1646 cm^{-1} carboxyl peak and 679 cm^{-1} Fe-O shift, suggesting interlayer exchange and Fe^{2+} coordination. Chlorite shows moderate enhancement at 1646 cm^{-1} but weak CMC fingerprint peaks, indicating parallel orientation adsorption. Apatite shows only faint carboxyl peaks with absent C-H characteristics, confirming weak adsorption.

3.2.4. XPS Analysis

XPS detection was performed on apatite, chlorite, and biotite before and after CMC-Na treatment.

(1) The XPS survey spectra of apatite, chlorite, and biotite surfaces before and after CMC-Na interaction are shown in Figures 21, 22, and 23.

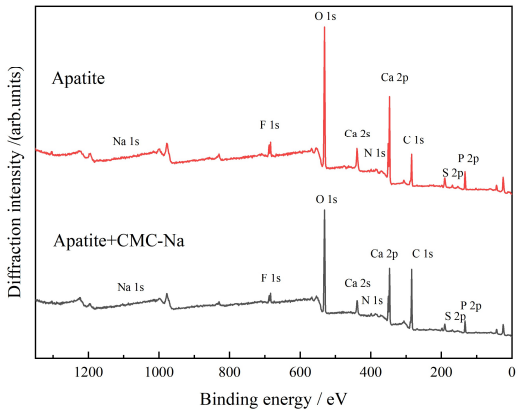

Figure 21. XPS survey spectra of apatite surface before and after CMC-Na interaction.

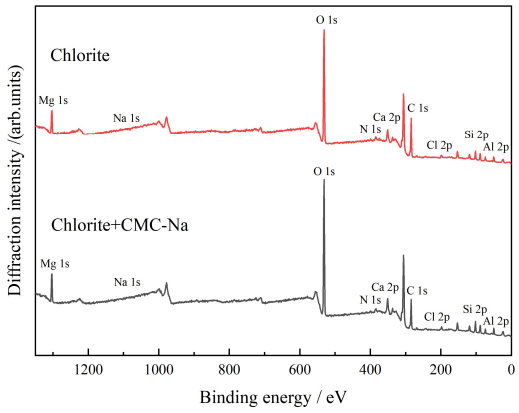

Figure 22. XPS survey spectra of chlorite surface before and after CMC-Na interaction.

 doi:10.20944/preprints202604.1645.v1

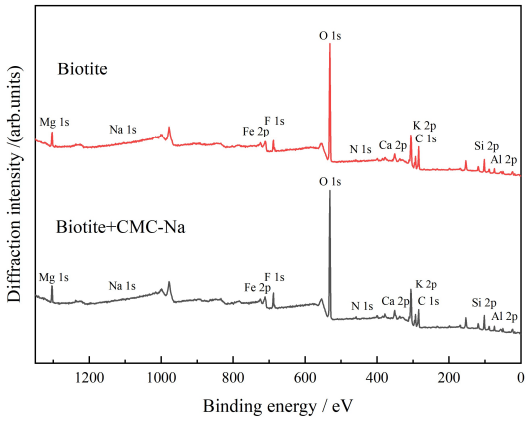

Figure 23. XPS survey spectra of biotite surface before and after CMC-Na interaction.

Figures 21, 22, and 23 indicate that CMC-Na coordinates with metal ions on mineral surfaces through its carboxyl groups (−COO^-) and forms hydrogen bonds through hydroxyl groups (−OH), thereby effectively coating the surfaces of all three minerals. This is directly reflected in the significant enhancement of carbon (C) signals in the XPS spectra. This process is a surface interaction that does not disrupt the bulk crystal structure of the minerals. Additionally, new nitrogen (N) signals were detected in some complexes by XPS, providing new clues for revealing deeper interaction mechanisms.

(2) Figure 24 presents the peak-fitting results of high-resolution C 1s spectra of the three minerals before and after CMC-Na treatment.

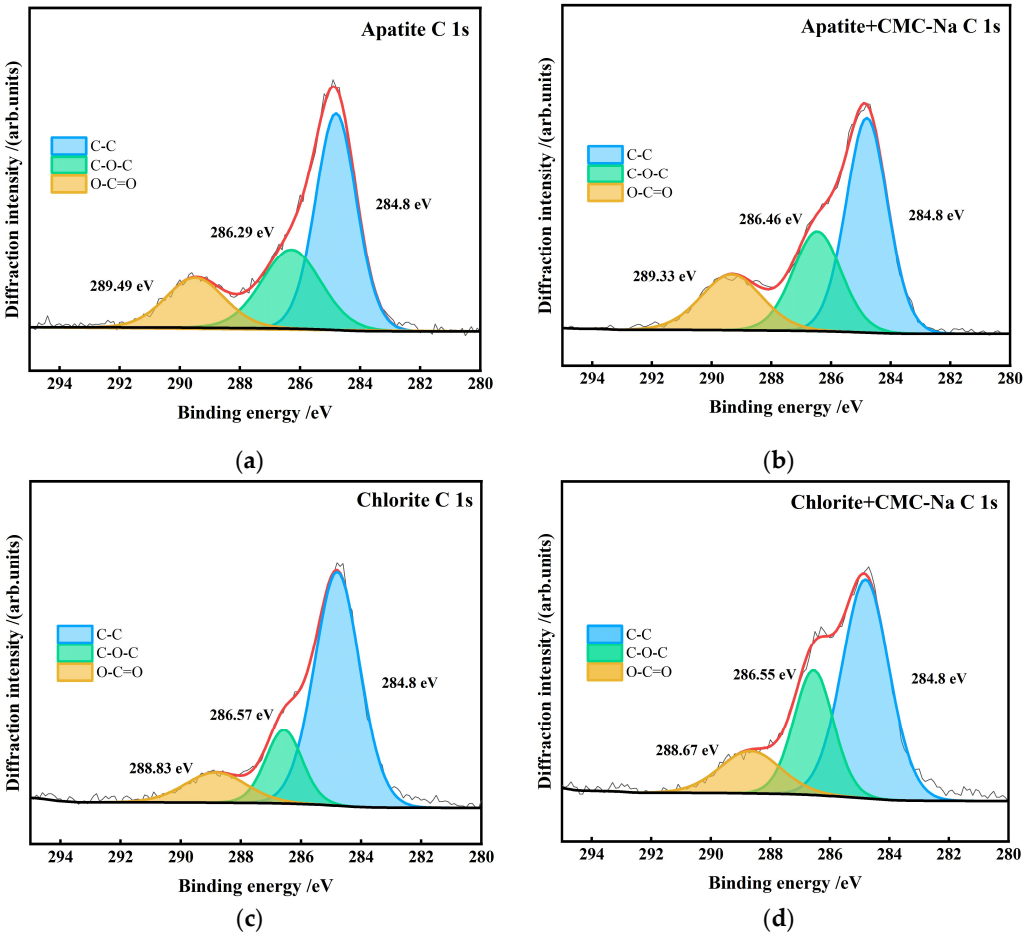

 doi:10.20944/preprints202604.1645.v1

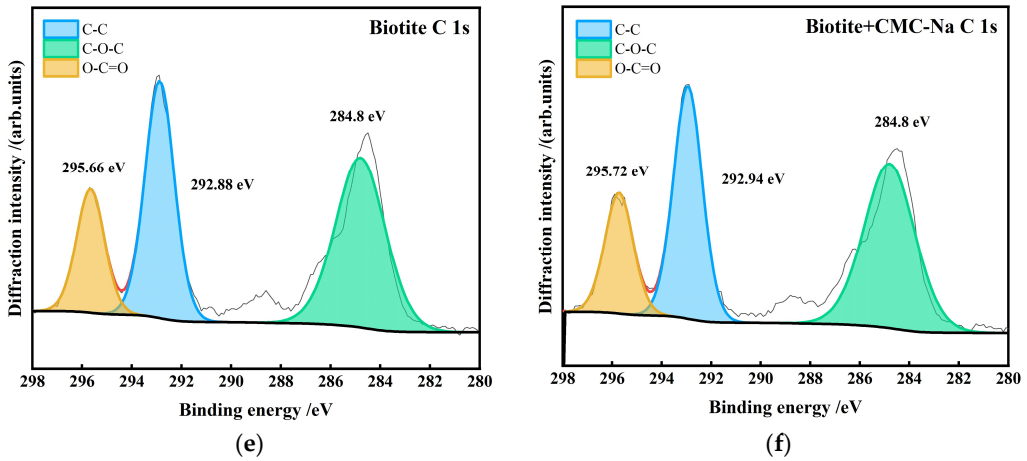

Figure 24. Peak fitting of C 1s spectra of mineral surfaces before and after CMC-Na interaction: (**a**) Apatite C 1s; (**b**) Apatite+CMC-Na C 1s; (**c**) Chlorite C 1s; (**d**) Chlorite+CMC-Na C 1s; (**e**) Biotite C 1s; (**f**) Biotite+CMC-Na C 1s.

Comprehensive analysis of FTIR spectra, XPS survey spectra, and high-resolution C 1s spectra indicates that CMC-Na undergoes specific coordination with metal ions on mineral surfaces through its carboxyl groups (−COO^-), with its macromolecular chains forming effective coating layers on the mineral surfaces. This process is a surface interaction that does not disrupt the bulk structure of the minerals. Apatite shows weak C signals with slight COO^- peak shift, indicating no strong interaction with CMC-Na. Chlorite exhibits negative COO^- peak shift, suggesting −COO^- coordination with Mg^{2+} and alteration of electron cloud density. Biotite shows slight positive −COO^- shift, indicating interlayer K^+ exchange with Na^+.

(3) The apatite surface is rich in Ca^{2+}, which exhibits strong chemisorption interaction with CMC-Na. Figure 25 presents the peak-fitting results of high-resolution Ca 2p spectra of apatite before and after CMC-Na treatment.

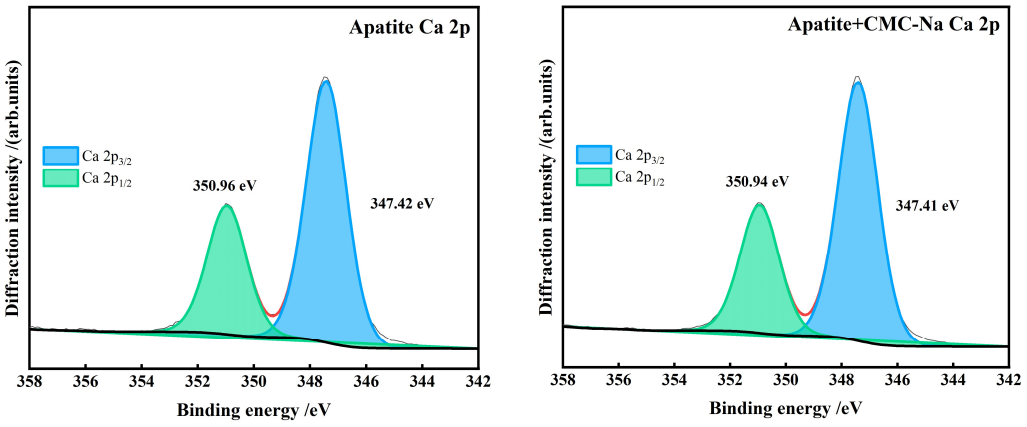

Figure 25. Peak fitting of Ca 2p spectra of apatite surface before and after CMC-Na interaction: (**a**) Apatite Ca 2p ; (**b**) Apatite+CMC-Na Ca 2p.

As shown in Figure 25, no significant changes are observed in the Ca $2p_3/_2$ (347.42 eV → 347.41 eV) and Ca $2p_1/_2$ (350.96 eV → 350.94 eV) peak positions before and after CMC-Na interaction, with the spin-orbit splitting energy maintained at 3.54 eV. This indicates that CMC-Na does not form chemical coordination bonds with lattice Ca^{2+} on the apatite surface, but only adsorbs through weak

 doi:10.20944/preprints202604.1645.v1

physical interaction. This constitutes the structural basis for the weaker depressing effect of CMC-Na on apatite compared to gangue minerals.

(4) Chlorite is a magnesium-bearing layered silicate mineral. CMC-Na can adsorb through interaction with Mg^{2+} in the interlayer or at edges, resulting in negative shift of the Mg 1s peak. Figure 26 presents the peak-fitting results of high-resolution Mg 1s spectra of chlorite before and after CMC-Na treatment.

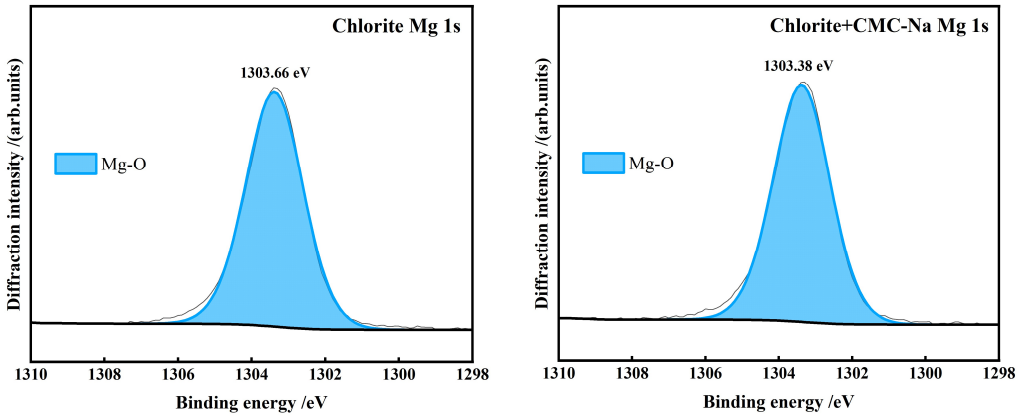

(**a**) (**b**)

Figure 26. Peak fitting of Mg 1s spectra of chlorite surface before and after CMC-Na interaction: (**a**) Chlorite Mg 1s ; (**b**) Chlorite+CMC-Na Mg 1s.

As shown in Figure 26, the binding energy of Mg 1s in chlorite decreases from 1303.66 eV to 1303.38 eV after CMC-Na interaction, with a negative shift of 0.28 eV, confirming the formation of chemical coordination bonds between the carboxyl groups of CMC and Mg^{2+} in the octahedral layer. In contrast to the unchanged Ca 2p of apatite, this demonstrates the selective chemisorption of CMC-Na on gangue minerals; however, the small contact angle change suggests parallel orientation of CMC, resulting in lower hydrophobic competition efficiency.

(5) Biotite is a potassium-bearing layered silicate mineral. The interlayer K^+ ions are highly active. Figure 27 presents the peak-fitting results of high-resolution K 2p spectra of biotite before and after CMC-Na treatment.

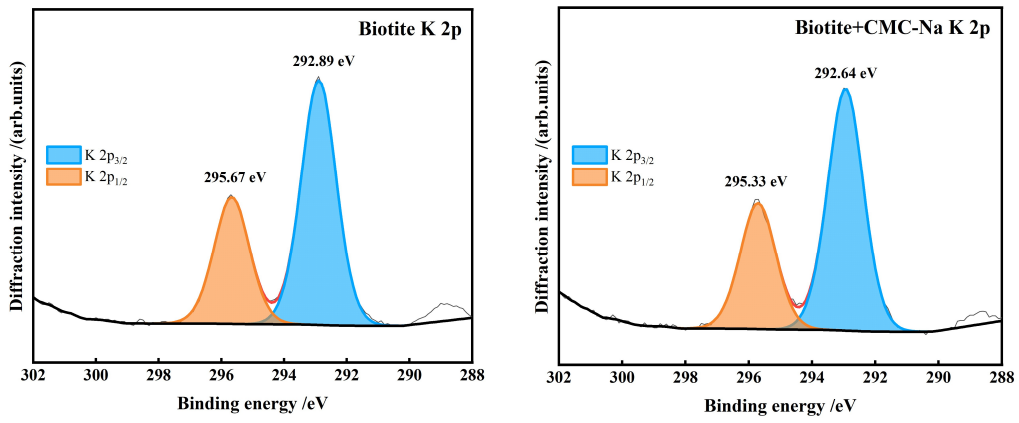

(**a**) (**b**)

Figure 27. Peak fitting of K 2p spectra of biotite surface before and after CMC-Na interaction: (**a**) Biotite K 2p ; (**b**) Biotite+CMC-Na K 2p.

 doi:10.20944/preprints202604.1645.v1

As shown in Figure 27, after CMC-Na interaction, the K $2p_{3/2}$ (292.89 → 292.64 eV) and K $2p_{1/2}$ (295.67 → 295.33 eV) peaks of biotite exhibit significant negative shifts, with the spin-orbit splitting energy decreasing from 2.78 eV to 2.69 eV. This confirms ion exchange between Na^+ and interlayer K^+ and the intercalation of CMC molecules into the interlayer space.

The above results confirm that CMC-Na selectively adsorbs onto gangue mineral surfaces through chemical coordination (chlorite) and interlayer intercalation (biotite), while having negligible effect on the target mineral apatite, thereby achieving selective depression for flotation separation.

4. Results

This study focuses on the challenge of separating layered silicate minerals (chlorite and biotite) from fine-grained apatite flotation. Systematic pure mineral flotation tests, artificial mixed mineral flotation tests, and mechanism studies were conducted. The main conclusions are as follows:

(1) Pure mineral and artificial mixed mineral flotation test results demonstrate that under the conditions of pH 9 and collector dosage of 5 kg/t, CMC-Na can effectively achieve selective separation of apatite from chlorite and biotite; however, the optimal depressing dosage exhibits a significant particle size effect. For the −0.5+0.074 mm size fraction, effective separation can be achieved with collector alone; for the −0.074+0.023 mm size fraction, 10–100 mg/L CMC-Na strongly depresses chlorite and biotite, with apatite recovery reaching 87%–41.8%; while for the −0.023 mm size fraction, effective separation requires 30–300 mg/L CMC-Na, where chlorite and biotite are strongly depressed and apatite recovery increases to 24.8%.

(2) Mechanism studies confirm that the significantly different adsorption behaviors of CMC-Na on the three mineral surfaces constitute the fundamental reason for achieving selective depression. Contact angle measurements indicate that CMC-Na substantially enhances the hydrophilicity of gangue minerals, with the contact angle of chlorite decreasing from 66.5° to 62.9° and biotite from 33.1° to 27.0°, whereas apatite only decreases from 85.7° to 75.3°, maintaining strong hydrophobicity. Zeta potential analysis shows that the adsorption strength of CMC-Na on gangue mineral surfaces is much greater than on apatite, with potential negative shifts following the order: biotite (−9.5 mV) > chlorite (−7.5 mV) > apatite (−4.0 mV).

(3) FTIR and XPS analyses jointly confirm that CMC-Na adsorption on all three mineral surfaces is dominated by the $—COO^-$ functional group. However, significant differences exist in adsorption strength and mechanism: on biotite surfaces, $—COO^-$ undergoes ion exchange with interlayer K^+ and coordinates with octahedral Fe^{2+}/Mg^{2+}, resulting in the strongest adsorption; on chlorite surfaces, $—COO^-$ forms chemical coordination bonds with octahedral Mg^{2+}, showing moderate adsorption; while on apatite surfaces, the inherent lattice Ca^{2+} interacts weakly with CMC-Na, primarily through weak physical adsorption. This differential adsorption ultimately leads to the excellent selective depression effect of CMC-Na on gangue minerals, providing an effective reagent regime and theoretical basis for fine-grained phosphate ore flotation separation.

 doi:10.20944/preprints202604.1645.v1

Author Contributions: M.L.: Investigation, data curation, conceptualization, methodology, writing—review & editing; L.Z.: Resources, writing—review & editing, funding acquisition; Z.Yi.: Data curation, validation; Z.Ya.: Data curation, validation; J.H.: Data curation, validation; B.G.: Resources, funding acquisition; M.H.: Resources, funding acquisition; W.L.: Resources, funding acquisition; Y.L.: Resources, funding acquisition; C.W.: Resources, funding acquisition; X.G.: Supervision. All authors have read and agreed to the published version of the manuscript.

Funding: This research was supported by the National Natural Science Foundation of China Youth Program (No. 51804123) and the Technology Development Entrusted Project of HBIS Group Co., Ltd. (Contract No. HG2022116).

Data Availability Statement: The original contributions presented in this study are included in the article. Further inquiries can be directed to the corresponding authors.

Conflicts of Interest: There are no conflicts of interest associated with this study.

Abbreviations

The following abbreviations are used in this manuscript:

CMC-Na Carboxymethyl Cellulose Sodium

References

1. Zhu, P.C.; LI, X.; LI, F.; Wei, J.X. Process mineralogy research and flotation experiment in a phosphate mine of Yichang. Mining Research and Development, 2018, 38, 85-88.
2. Dong, L.Y., Cui, Y.R., Qiao, L.D. A critical review on the flotation of calcium-containing minerals. Separation and Purification Technology, 2025, 360, 131082.
3. Liu, Y.; Wu, Z.X.; Tao, D.P. Experimental Study on Reverse Flotation Desilication of Phosphate Using a Novel Cationic Collector. Mining Research and Development, 2026, 46, 291-300.
4. Xue, K.; Zhang, R.Y. Advances of researches on the distribution and metallogenic characteristics of phosphorous deposits in China. Acta Mineralogica Sinica, 2019, 39, 7-14.
5. Yin, W.Z. Progress in research on mineral flotation interaction effects. Nonferrous Metals (Mineral Processing Section), 2024, 1-12, 56.
6. Jia, Y.K.; Yao, J,; Yin, W.Z.; Yang, P. Ultrasonic Regulation of the Interaction Mechanism Between Hematite and Chlorite During Flotation. Metal Mine, 2025, 09, 107-113.
7. Peng, L.Q.; Liu, R.Z.; Li, R.L.; Zhang, C.W.; Luo, K.Y.; Zhang, C.The scrubbing-flotation research on collophanite with higher silica and sesquioxide content. Yunnan Chemical Technology, 2024, 51, 69-71.
8. Guo, Y.J.; Li, j.l.; Fan, P.Q.; Li, H.B.; Chen, C.Y.; Du, L.P.; Xu, S.Experimental Study on a New Process of Classification Flotation Desilication of Phosphogypsum in Yunnan. Non-Metallic Mines, 2022, 45, 53-56.
9. Huang, G.; Xu, H.X.; Ma, L.Q.; Lun, W. Improving coal flotation by classified conditioning. International Journal of Coal Preparation and Utilization, 2018, 38, 361-373.
10. Ruan, Y.Y.; Zhou, J.H.; Zhou, F.; Luo, H.H.; Wang, X.L.; Chi, R.A.; Deng, N.B.Study on process mineralogy characteristics and mixed reverse flotation test of Houping phosphate rock in Hubei. Industrial Minerals & Processing, 2026, 55, 1-7.
11. Che, Y.H.; Chen, W.; Zhu, Y.Y.; Qi, J.; Zhao, G.; Yang, L. Review on the Research Progress of Regulators Towards Clay Mineral Flotation. Metal Mine, 2023, 36-49.
12. Du, L.P.; Chen, C.Y.; ,Zhong, J.; Guo, Y.J. Brief analysis of phosphate beneficiation technology progress and problem countermeasures. Chemical Minerals & Processing, 2016, 45, 57-61.
13. Zhang, Q.; Mao, S.; Huang, X.F.; Chen, A.A.; Zhang, W.B. Research progress in surface chemistry of flotation for apatite and gangue minerals in phosphate ore. Mineral Protection and Utilization, 2024, 44, 1-15.
14. Dankwah, J.B.; Asamoah, R.K.; Zanin, M.; Skinner, W.Dense liquid flotation:Can coarse particle flotation performance be enhanced by controlling fluid density. Minerals Engineering, 2022, 180, 107513.

 doi:10.20944/preprints202604.1645.v1

15. Fatemeh, K.; Ataallah, B.; Yousef, G.; Abolfazl, D.; Morteza, A.; Hadi, F.; Mohsen, H. The interaction and synergic effect of particle size on flotation efficiency: A comparison study of recovery by size,and byliberation between lab and industrial scale dana. Rudarsko-geološko-naftni zbornik, 2023, 38, 1-12.
16. Meftuni, Y.; Sonmez, I. Effect of the hydrophobic fraction and particle size in the collectorless column flotation kinetics. Colloids and Surfaces A:Physicochemical andEngineering Aspects, 1997, 121, 9-13.
17. Cheng, H.Z.; Zhang, B. Course of development of fine coal flotation process in China. Coal Preparation Technology, 2024, 52, 56-61.
18. Meng, C.; Li, L.X.; Shen, S.P.; Qi, S.L.; Yu, J.; Yuan, Z.T. Experiments on classified magnetic separation-classified flotation for a ilmenite. Mineral Protection and Utilization, 2017, 59-63.
19. He, H.T.; Zhang, H.; Yang, W.Q.; Cai, Z.J. Effect of particle size on the desilication of Kunyang Yunnan collophonite by reverse flotation. Yunnan Chemical Industry, 2021, 48, 32-34.
20. Li, Y.H.; Liu, H.; Yang, B.Q.; Zeng, M.Y.; Zhang, H.Q.; He, G.S.; Luo, H.H. Application and its mechanism of sodium lignosulfonatein in magnesium removal from phosphate ore by direct flotation.Nonferrous Metals (Mineral Processing Section), 2023, 3, 152-157.
21. Li, Z.H.; Xiong, K.; Zuo, K.S.; Gao, P. Effect of Carboxymethyl Cellulose on Flotation of Ascharite/Serpentine and Its Action Mechanism. Metal Mine, 2024, 10, 107-111.
22. Hu, Y.W.; Wang, L.; Wang, J.L.; Cao, Z.; Liu, L.; Li, G. Influences and Mechanisms of Carboxymethyl Cellulose on the Flotation Behavior of Columbite and Ankerite. Nonferrous Metals (Mineral Processing Section), 2025, 11, 109-119.
23. Wu, H.B. Adsorption behavior and mechanism of cellulose inhibitors in the system of scheelite flotation. Master's Thesis, Jiangxi University of Science and Technology, Ganzhou, China, 2018.
24. Zhang, W.P. Effects of macromolecular organic depressants on flotation behavior of apatite and calcium carbonate minerals and the mechanism. Master's Thesis, Jiangxi University of Science and Technology, Ganzhou, China, 2020.
25. Ma, Q.; Li, Y.B.; Li, W.Q.; Yang, X. Study on the reaction mechanism of fluorite and calcite flotation separation by carboxymethyl cellulose. Metal Mine, 2022, 7, 187-192.
26. Guo, F.; Li, J. Separation strategies for Jordanian phosphate rock with siliceous and calcareous gangues. Mineral Processing, 2010, 97, 74-78.
27. Lópze-valdivieso, A.; Lozano-ledesma, L.A.; Robledo-cabrera, A. Orozco-Navarro, O.A. Carboxymethylcellulose (CMC) as PbS depressant in the processing of Pb-Cu bulk concentrates:Adsorption and floatability studies. Minerals Engineering, 2017, 112, 77-83.
28. Zhang, H.; Li, H.B.; Zhao, F.T.; Yang, W.Q.; Liu, R.Z. Study and application of determination method of contact angle of phosphate powder. Chemical Minerals & Processing Matters, 2020, 49, 22-24.
29. Huang, X.F.; Gong, F.Z. Measurement of contact angles of solid powder by Washburn osmotic pressure method. Laboratory Research and Exploration, 2003, 5, 48-50.
30. Wang, J.L.; Wang, J.L.; Shi, J.Y.; Wu, X.; Cao, Z. Research progress on surface property testing methods for mineral flotation. Minerals Protection and Utilization, 2025, 45, 101-113.